

Tribological Properties of Nanometric Atomic Layer Depositions Applied on AISI 420 Stainless Steel

E. Marin^a, A. Lanzutti^a, L. Fedrizzi^a

^aUniversity of Udine, Department of Chemistry, Physics and Environment, Via del Cottonificio 108, 33100 Udine, Italy.

Keywords:

Surfactants
Self-assemble
Boundary lubrication
Nanotechnology

Corresponding author:

E. Marin
University of Udine,
Department of Chemistry,
Physics and Environment,
Via del Cottonificio 108,
33100 Udine,
Italy.
E-mail: elia.marin@uniud.it

ABSTRACT

Atomic Layer Deposition (ALD) is a modern technique that allows to deposit nanometric, conformal coatings on almost any kind of substrate, from plastics to ceramic, metals or even composites. ALD coatings are not dependent on the morphology of the substrate and are only regulated by the composition of the precursors, the chamber temperature and the number of cycles.

In this work, mono- and bi-layer nanometric, protective low-temperature ALD coatings, based on Al₂O₃ and TiO₂, were applied on AISI 420 Stainless Steel in order to enhance its relatively low corrosion resistance in chloride containing environments. Tribological testing were also performed on the ALD coated AISI 420 in order to evaluate the wear and scratch resistance of these nanometric layers and thus evaluate their durability.

Scratch tests were performed using a standard Rockwell C indenter, under a variable load condition, in order to evaluate the critical loading condition for each coating. Wear testing were performed using a stainless steel counterpart, in ball-on-disc configuration, in order to measure the friction coefficient and to confront the wear resistance. All scratch tests scars and wear tracks were then observed by means of Scanning Electron Microscopy (SEM) in order to understand the wear mechanisms that occurred on the sample surfaces.

Corrosion testing, performed under immersion in 0.2 M NaCl solutions, clearly showed that the ALD coatings have a strong effect in protecting the Stainless Steel substrate against corrosion, reducing the corrosion current density by two orders of magnitude. The preliminary tribological results showed that ALD depositions obtained at low temperatures have a brittle behavior caused by the amorphous nature of their structure, and thus undergo delamination phenomena during Scratch Testing at relatively low applied loads. During ball-on-disc testing, the coatings were removed from the substrate, in particular for monolayer ALD configurations, which seem to have a lower toughness when compared to bi-layer configurations.

© 2013 Published by Faculty of Engineering

1. INTRODUCTION

Martensitic stainless steels are widely used for a wide range of applications, mainly due to their

balanced properties, as they couple relatively microhardness, mechanical resistance and corrosion resistance in many aggressive environments [1]. For these reasons, martensitic

stainless steels are nowadays applied for: knife blades [2], oil and gas [3], offshore platforms [4], turbine blades [5], components subject to abrasive wear at relatively high temperature or aggressive environments [6].

Even so, stainless steels could show insufficient corrosion resistance in strongly aggressive media containing Cl^- and S^{2-} ions, at high temperature or very high / low pH values [7]. For these reasons, in particular circumstances Stainless Steels may need a further improvement of corrosion protection. Conventional treatments, such as painting, are hardly applicable to Stainless Steel due to adhesion problems between paint and the metal substrate [8].

A great number of innovative treatments are nowadays under intensive study to improve Stainless Steel corrosion resistance, such as plasma detonation techniques [9], arc-ion plating [10], sol-gel deposition [11], chemical conversion layers of cerium [12] chromium [13] or other elements, Chemical Vapor Deposition [14], High-Velocity Oxy-fuel Spray (HVOF) [15], plasma-nitriding [16], and Atomic Layer Deposition [17]. All these techniques may also be applied in order to improve the tribological resistance of the substrate, as they grant higher hardness and wear abrasion when compared to stainless steel or other common metallic alloys [18-21].

The modern concept of ALD is an extension of the ALE (Atomic Layer Epitaxy), patented by Prof. Suntola [22]. Suntola's studies were mainly focused on switching effects in chalcogenide nanometric films for solid state electronic devices [23-25], and lately extended to a wide range of amorphous semi-conductive thin films [26]. ALD (as ALE) process involves a sequence of self-limiting surface reactions. As evidenced in 1980 by Ahonen et al. [27], the self-limiting characteristic of each reaction step differentiates ALE and ALD from other chemical vapor deposition technologies. In ALD each deposition cycle is clearly divided in four steps: in the first step a precursor is injected in the deposition chamber. The precursor is chosen so that its molecules will not react with each other at the deposition temperature. In ideal situations, a single monolayer is thus formed as a result of the reaction with the substrate. In the second step, the chamber is purged with nitrogen or argon gas in order to remove the excess of reactant and prevent "parasitic" CVD deposition on the substrate, which

will eventually occur if two different precursors are present in the deposition chamber at the same time. In the third step, the second precursor is injected in the chamber. In the case of metal oxide layers, this is an oxidant agent, usually simple H_2O . The last step of the deposition cycle is a second purge to remove the excess of reactant with purging gas. Closed-loop repetitions of the four basic steps theoretically allow obtaining perfectly conformal deposits of any desired thickness. By avoiding the contact between the precursors throughout the whole coating process, a film growth at atomic layer control, with a thickness control within ~ 10 pm, can be obtained.

Interest in ALD has increased stepwise in the mid-1990's and 2000's, with the interest focused on silicon-based microelectronics [28]. Up to the present time, ALD processes have been used to deposit several types of nanometric films, including several chemical compounds (e.g. AsGa, CdSe,...), metal oxides (e.g. Al_2O_3 , CaO, CuO, Er_2O_3 , Ga_2O_3 , HfO_2 , La_2O_3 , MgO, Nb_2O_5 , Sc_2O_3 , SiO_2 , Ta_2O_5 , TiO_2 , Y_2O_3 , Yb_2O_3 , ZnO, ZrO_2), nitrides (e.g. TiN, TaN, AlN, GaN, WN, NbN), sulfides (e.g. SrS, ZnS), carbides (e.g. TaC, TiC), fluorides (e.g. CaF_2 , LaF_3 , MgF_2), pure metals (e.g. Ru, Ir, Ta, Pt), biomaterials (e.g. hydroxyapatite ($\text{Ca}_{10}(\text{PO}_4)_6(\text{OH})_2$)) and even polymers (e.g. Polyimides) [29,30].

Results on the corrosion protection on stainless steel by ALD TiO_2 and Al_2O_3 layers were already obtained by Matero et al. (1999) [30], which supposed that the conformal ALD coatings could improve the corrosion resistance of different metal alloys. In 2007, Shan et al. [31] used TiO_2 ALD layers to protect an undefined stainless steel, obtaining only a limited effect. In 2011, Marin et al. [32], Diaz et al. [17] and Potts et al. [33] clearly showed that the residual porosity of ALD layers decreases increasing the thickness of the layer thus improving the protection of the substrate. In most cases [32,17,33,34] the nanometric ALD layers clearly showed a corrosion protection similar, if not superior to conventional protective techniques and thicker coatings, even if common industrial tests (salt spray) performed on Plasma Enhanced ALD by Potts et al. [33] clearly showed a time-limited corrosion protection.

In this work, characterization of ALD coated AISI 316 L has been carried out, in order to determine the possible use of nanometric ceramic ALD coatings for the corrosion and tribological protection of stainless steel.

2. EXPERIMENTAL

2.1 Samples production

Discs of standard AISI 420 martensitic stainless steel (chemical composition wt. %: C = 0.035; P < 0.04; S < 0.03; Mn = 2.0; Si = 0.75; Cr = 16.0 – 18.0; Ni = 10.0 – 15.0; Mo = 2.0 – 3.0) were obtained by machining and cutting of bars. The discs were then grinded using SiC abrasive paper in order to obtain a surface roughness of about 100 nm Ra, which was considered to be suitable for testing, in particular in the case of Glow Discharge Optical Emission Spectrometry (GDOES) analyses and wear. Samples surface was then cleaned using ethanol in ultrasonic bath for 10 minutes and dried in a dry heat sterilizer at a temperature of 80° C for 15 minutes. Some samples were then partially masked with heat resistant laboratory tape to prevent ALD deposition on part of the substrate, thus creating a clear and sharp interface between coated and uncoated region after adhesive tape removal.

The ALD coating was deposited using a TFS 500 reactor (Beneq Oy, Finland): Al₂O₃ layers were obtained using trimethylaluminium (Al(CH₃)₃) and H₂O precursors and TiO₂ layers were obtained using titanium tetrachloride (TiCl₄) and H₂O precursors. Both depositions were performed at a temperature of 120 °C. The low temperature processes were chosen in order to obtain an amorphous structure for both layers. The number of precursor cycles for each deposition was calculated using a growth rate per cycle (GPC) of ~0.1 nm/cycle for TiO₂ and a GPC of ~0.15 nm/cycle for Al₂O₃.

The samples were coated using different ALD configurations, with an overall coating thickness of about 200 nm.

2.2 Morphology

Morphological characterization was carried out using Veeco's Digital Instrument's Nanoscope IIIa atomic force microscope (AFM) in tapping mode configuration, using a Bruker SCM-PIT tip (Antimony (n) doped Si, frequency: 60-100 kHz, elastic constant: 1-5 N/m, PtIr coated) and Carl Zeiss EVO-40 scanning electron microscope (SEM) with an operating voltage of 20 kV. Analyses were performed on the stainless steel substrate and on coated samples. In particular, SEM was used in

order to scan the surface of the sample and investigate the presence of deposition defects and/or surface anomalies. AFM was mainly used to investigate the presence of surface morphological defects on the coating that were supposed to be hardly visible using SEM due to the coating transparency. AFM was also used at the interface regions between coated and uncoated substrate after adhesive tape removal in order to obtain information about the overall thickness of the deposits and confront it with the theoretical deposition rates values and the results obtained from GDOES analyses.

2.3 Composition

In-depth compositional analyses were carried out using Horiba Yobin-Yvon's RF – GD Profiler GDOES. Due to the difficulties in calibration of GDOES for the analysis of Titanium and Aluminum oxides, only qualitative compositional analyses were performed, even if a keen calibration was performed in order to obtain reliable single layer thickness values. GDOES technique is strongly influenced by surface roughness, which was relatively high.

2.4 Mechanical properties

In order to evaluate the resistance to delamination of the different ALD configurations, Vickers indentations were applied to the samples under different load conditions (HV0.1-0.2-0.5-1.0-2.0) and the delaminated areas have been then measured using a specific image post-processing software (Wayne Rasband, ImageJ 1.44p). As all indentation hardness tests, Vickers indentation are dependant from the mechanical characteristics of the substrate and can only be used to compare different coatings applied on the same substrate and not results from different substrates. As adhesion is strictly connected to the surface roughness [34-36], Vickers adhesion tests will give reliable results only for substrates with similar surface finishing.

2.5 Electrochemical properties

Electrochemical characterization of the different samples was performed using Potentiodynamic Polarizations. An AUTOLAB PGSTAT-20 potentiostat was used in a standard three electrodes configuration. The reference electrode was Ag/AgCl and the counter electrode was a

99.99% pure Platinum wire. All measurements have been performed in a pH 6.5, 0.2 M solution of NaCl. All polarization curves were obtained using a scan speed of 0.2 mV/s after 10 minutes of immersion of the samples, in order to stabilize the OCP. The potential has been increased from -200 mV respect to the OCP to a measured current density of about 10^{-3} A/cm².

2.6 Wear properties

Wear properties were investigated using an industrial CETR UMT tribometer in ball-on-disc configuration [37], using a WC counter-material. Wear testing was performed for 1, 10 and 100 cycles under dry conditions, at a relatively low rotating speed (1 rps) and at different diameters (15 mm, 18 mm, 21 mm). After testing, the wear tracks were observed using SEM and the volume losses were then estimated using a stylus profilometer.

3. EXPERIMENTAL RESULTS

3.1 Morphology

SEM resulted to be an inadequate technique for the analysis of ALD layers, since no morphological differences were found between images obtained on coated and uncoated regions and no morphological properties of the ALD layers could be correctly resolved using this technique, even at relatively high magnifications, such as 20k or 50k.

Figure 1 shows the SEM image obtained on the Al₂O₃ coated samples, at relatively “low” (Fig. 1a) and “high” (Fig. 1b) magnifications. It is only possible to discriminate the presence of scars and scratches caused by the cutting and grinding of the stainless steel substrates, while no information about the presence of the ALD layer could be obtained from these images.

Similar results were obtained in the case of the Al₂O₃/TiO₂ coated samples, at relatively “low” (Fig. 2a) and “high” (Fig. 2b) magnifications. It can be observed that, even for this sample, only scars and scratches caused by the mechanical cutting and grinding of the sample can be observed.

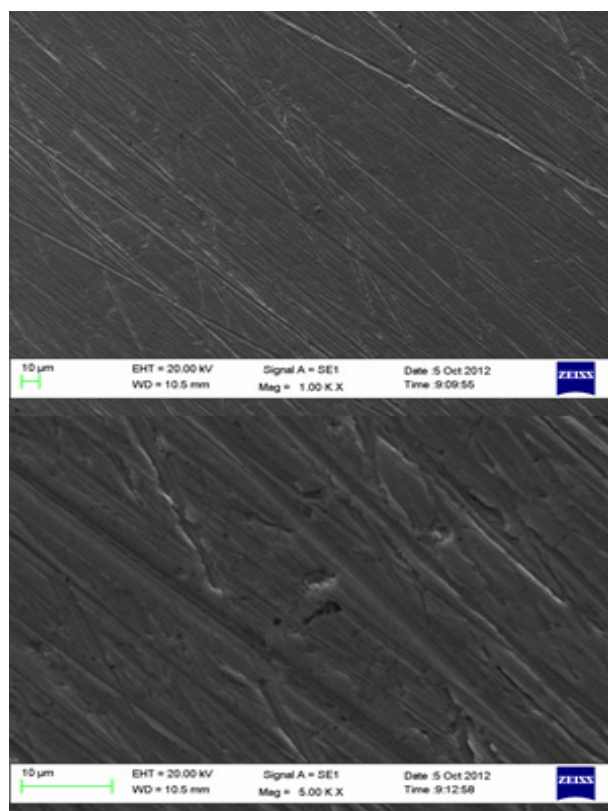


Fig. 1. SEM images of Al₂O₃ coated sample obtained at 1000 (a) and 5000 (b) magnifications.

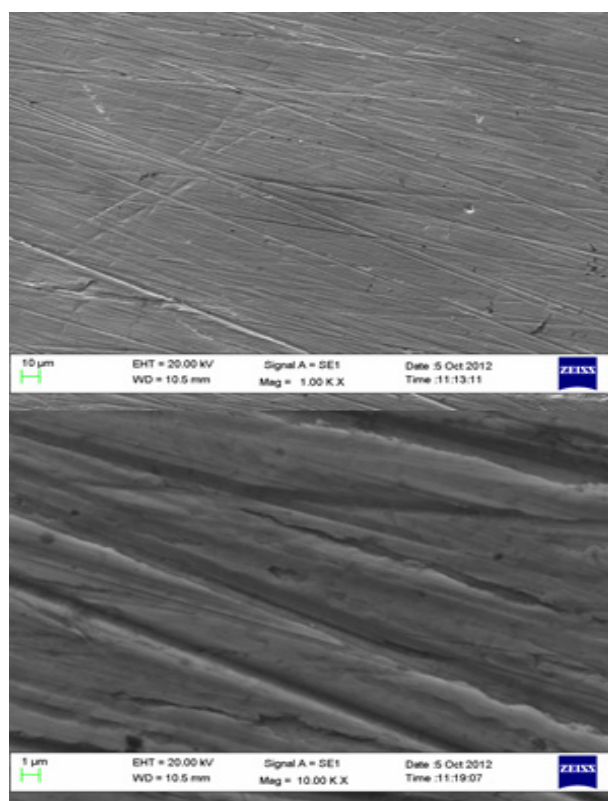


Fig. 2. SEM images of Al₂O₃ coated sample obtained at 1000 (a) and 5000 (b) magnifications.

AFM observations gave similar results, with only scratches and scars clearly visible on the morphological maps obtained. In the case of the maps obtained at the interface between coating and substrate, they were successfully used in order to estimate the overall coating thickness of the different ALD layers (Fig. 3).

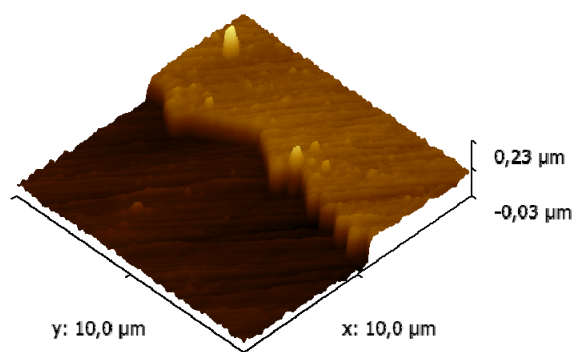


Fig. 3. AFM image obtained at the interface between coated and uncoated areas of the Al₂O₃ coated sample.

The results obtained are resumed in Table 1:

Table 1. Coating thickness as obtained by AFM measurements.

Coating	Thickness
	μm
Al ₂ O ₃	102 ± 3
Al ₂ O ₃ /TiO ₂	107 ± 5

a. Composition

GDOES thickness measurement accuracy was strongly influenced by the sharpness of the interface region between coating and substrate. Conventionally, in this work the coating thickness has been measured between the top surface and the intersection point between oxygen and iron signals. Since no reference materials were present for amorphous ceramics, a specific GDOES calibration was required. Sputtered crater's depth was measured using a stylus profilometer and the sputtering rate has been evaluated accordingly. Following this calibration GDOES results shall be considered semi-quantitative and for this reason the composition of the coatings and in particular of Al₂O₃ layers is not stoichiometric.

Fig. 4 shows the results obtained by GDOES on the Al₂O₃ coated sample. It can be observed that the interface between coating and substrate is not sharp. This is caused by the relatively high surface roughness obtained after the sample preparation. The iron signal, which is considered representative for the substrate, reaches a plateau at about 200 nm, which is influenced by

both coating thickness and surface roughness, meaning that, after 200 nm, only substrate signals can be seen by GDOES. At about 75 nm, the two signals of Iron and Oxygen are even, while at the surface, both Oxygen and Aluminium show a peak. This behaviour is caused by the substrate roughness, which causes a strong signal overlap. For this reason, coating thickness could not be correctly estimated using GDOES, but only the thickness range could be determined. Surface peak in oxygen content can also be explained considering the well known hydrogen effect [38].

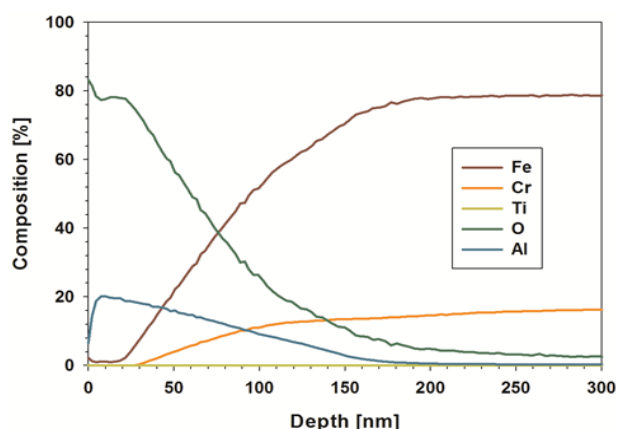


Fig. 4. GDOES graph obtained for the Al₂O₃ coated sample. Signals of Iron, Chromium, Titanium, Oxygen and Aluminium.

In the case of the bi-layer formed by a layer of Al₂O₃ followed by a second layer of TiO₂, both signals of Ti and Al can be observed in the first 150-200 nm of analysis, while Oxygen can be observed for more than 300 nm. The Iron signals show a plateau after about 170 nm. It can be observed that Titanium and Aluminium have a clear peak in the coating region. The titanium signals can be observed up to 100 nm, while the Aluminium signals can be observed up to 170 nm.

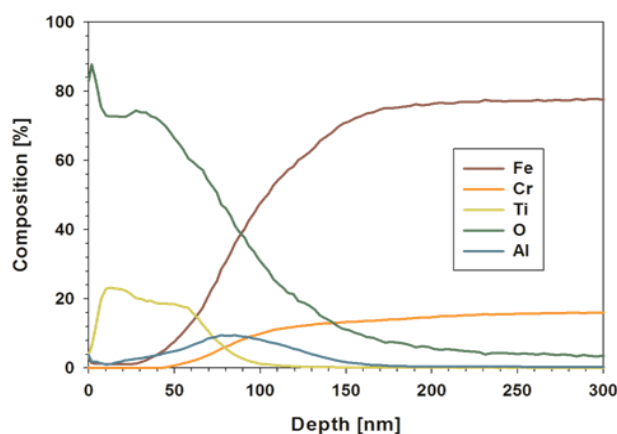


Fig. 5. GDOES graph obtained for the Al₂O₃ coated sample. Signals of Iron, Chromium, Titanium, Oxygen and Aluminium.

b. Mechanical properties

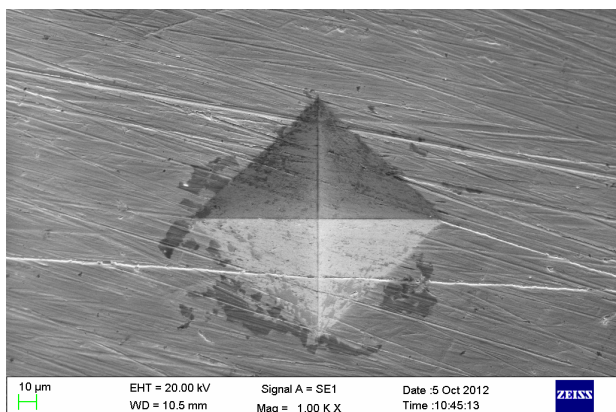


Fig. 6. 3 N Vickers indentation on AISI 420 Stainless Steel coated with Al₂O₃.

Vickers indentations performed on the coated sample surface were observed using SEM, as the Optical Microscope field depth resulted to be too small to sharply resolve all the delamination details on the deformed region in just one image. The dimension of the Vickers indentation is related to the applied load. Even if localized defects are hardly visible on the ALD coatings due to their transparency, larger areas with a complete coating removal resulted to be clearly visible on the SEM images. A clear example of how the delaminated areas have been evaluated is presented in Fig. 6 and Fig. 7. Fig. 6, in particular, shows a Vickers indentation as obtained using a 3 N load on the 100 nm TiO₂ coated sample, while Fig. 7 shows details of cracks and delamination obtained using a 10 N load. The results obtained for the different samples are plotted in Fig. 8, as a function of the applied load.

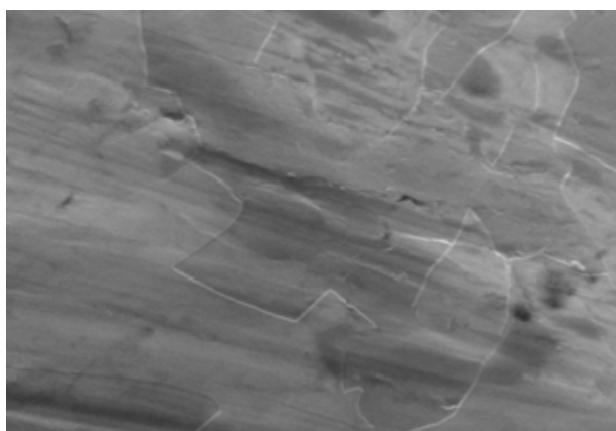


Fig. 7. Cracks and delamination in proximity of a Vickers indentation (5N on Al₂O₃ coated AISI 420).

All coatings showed a clear dependence on the applied load for the delaminated Area/Load ratio, which remains almost constant only at the

highest indentation loads (9.8 N = HV1 and 19.6 N = HV2).

It can be observed that the best behaviour is shown by the coating formed by two different layers, with a lower delamination, in particular at low loading conditions. At high loading conditions, and in particular at 19.6 N, the two coatings showed almost the same delamination areas.

Data dispersion was considerably high so a statistical approach was followed, with about 20 Vickers indentations per load for each sample.

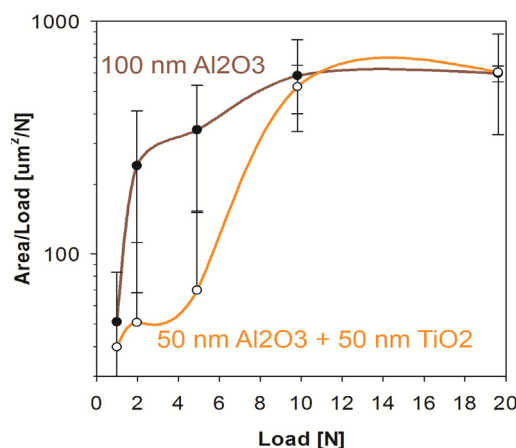


Fig. 8. Delamination as a function of the indentation load.

c. Electrochemical properties

Polarization curves for the different samples with a total coating thickness of about 100 nm are shown in Fig. 9. Uncoated AISI 420 clearly shows a passive behaviour in the 0.2 M NaCl solution, with a corrosion current density between 10⁻⁶ and 10⁻⁷ A/cm² and a passive region from -0.25 to -0.1 V with respect to Ag/AgCl. The Open Circuit Potential (OCP) for uncoated AISI 316 L steel resulted to be about 0.1 V with respect to Ag/AgCl.

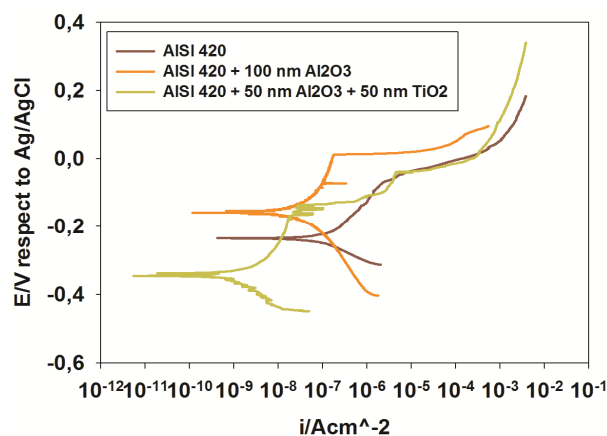


Fig. 9. Polarization curves obtained on both coated samples and on naked substrate.

The two coatings showed two different shifts of the corrosion potential, a positive shift to about -0.15 V respect to Ag/AgCl in the case of the single layer Al₂O₃ coating and a negative shift to about -0.35 V in the case of the bi-layered structure of Al₂O₃ and TiO₂.

In the case of the single layer coating, a corrosion current density reduction of about one order of magnitude, to about 3*10⁻⁸ A/cm², was observed, while in the case of the bi-layered structure, the corrosion current density reduction resulted to be more intense, reaching 3*10⁻⁹ A/cm².

In the case of the single layer coating, the barrier effect resulted to be similar in extension to the passive range of the naked AISI 420 substrate, at lower currents, while an extended barrier effect was observed in the case of the bi-layered structure.

d. Wear properties

Figure 10 shows the wear track obtained after 10 cycles of ball-on-disc wear testing on the sample coated with a single layer of Al₂O₃. It can be observed that, even if the applied load is relatively low, a wear track is clearly visible on the surface of the sample and, in particular, third body wear scars can be observed. The pristine surface roughness of the sample has been completely removed from the surface due to the tribological contact with the WC counter-part.

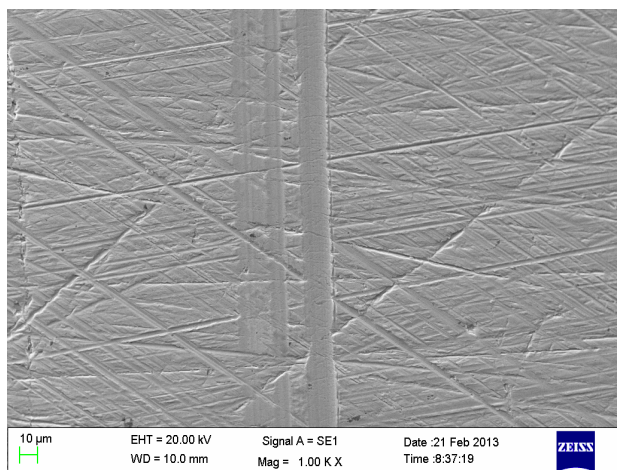


Fig. 10. Wear track obtained after just 10 cycles for Al₂O₃ single layer.

EDXS localized analysis shown that the ALD layer has been completely removed from the surface due to the tribological contact.

It is possible that the clearly visible third body wear on the surface of the sample has also been

caused by Al₂O₃ particles detached from the sample surface during testing.

Increasing the number of cycles, it was possible to observe the formation of a thick oxide layer inside the wear track, and strong adhesion phenomena, leading to a coarse wear track full of irregular oxide depositions.

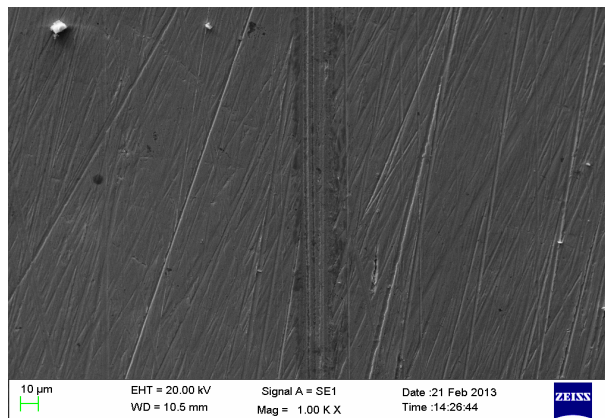


Fig. 11. Wear track obtained after just 10 cycles for Al₂O₃/TiO₂ bi-layer.

Fig. 11 shows the wear track obtained after 10 cycles of ball-on-disc wear testing on the sample coated with a bi-layer formed by Al₂O₃ and TiO₂.

It can be observed that, as seen before for the single layer sample, the wear track is clearly visible at 1000 magnifications. Scars of third body wear are present inside the wear track, even if the track itself is smaller when compared to the track obtained from the single layer sample.

Even in this case, EDXS analyses shown that the ALD layer has been completely removed from the wear track on the sample surface, due to the tribological contact with the WC counterpart.

4. CONCLUSIONS

Nanometric ALD mono- and bi- layers, with a total thickness of about 200 nm, were successfully applied to AISI 420 martensitic stainless steel using a thermal ALD process based on H₂O, TMA and TiCl₄.

The applied ALD layers and the substrate were successfully characterized using SEM, AFM, GDOES, stylus profilometer, electrochemical equipment and an industrial tribometer in ball-on-disc configuration.

The morphological characterization evidenced that ALD layers are conformal and almost defect-free even at relatively high magnifications.

GDOES testing correctly discriminated the presence of the different ceramic layers on the AISI 420 substrate.

Adhesion testing showed that adhesion between AISI 420 and 200 nm ALD layers is relatively poor and cracks propagate from microhardness Vickers indentations.

Electrochemical testing clearly showed that even an ALD coating with a limited thickness of about 200 nm is sufficient to strongly improve the corrosion resistance of the martensitic stainless steel substrate, strongly reducing the corrosion current densities and widening the passive range of this material.

Wear testing results showed that ALD layers deposited at the temperature of 120 °C on martensitic stainless steel, are unable to grant tribological resistance to the substrate, due to their intrinsic brittleness and the relatively low hardness of the substrate on which they were applied.

REFERENCES

- [1] H. Zhang, Y.L. Zhao, Z.D. Jiang: *Effects of temperature on the corrosion behavior of 13Cr martensitic stainless steel during exposure to CO₂ and Cl⁻ environment*, Materials Letters, Vol. 59, No. 27, pp. 3370-3374, 2005.
- [2] P.J. Hidalgo: *Pitting corrosion of martensitic cutlery steels*, Surface Technology, Vol. 10, No. 3, pp. 193-208, 1980.
- [3] A. Turnbull: *Modelling of environment assisted cracking*, Corrosion Science, Vol. 34, No. 6, pp. 921-960, 1993.
- [4] Y. Xi, D. Liu, D. Han: *Improvement of corrosion and wear resistances of AISI 420 martensitic stainless steel using plasma nitriding at low temperature*, Surface and Coatings Technology, Vol. 202, No. 12, pp. 2577-2583, 2008.
- [5] D. Ferreno, J.A. Alvarez, E. Ruiz, D. Mendez, L. Rodriguez, D. Hernandez: *Failure analysis of a Pelton turbine manufactured in soft martensitic stainless steel casting*, Engineering Failure Analysis, Vol. 18, No. 1, pp. 256-270, 2011.
- [6] B. Fournier, M. Sauzay, C. Caes, M. Noblecourt, M. Mottot, A. Bougault, V. Rabeau, J. Man, O. Gillia, P. Lemoine, A. Pineau: *Creep-fatigue-oxidation interactions in a 9Cr-1Mo martensitic steel. Part III: Lifetime prediction*, International Journal of Fatigue, Vol. 30, No. 10-11, pp. 1797-1812, 2008.
- [7] C. Liu, G. Lin, D. Yang, M. Qi: *In vitro corrosion behavior of multilayered Ti/TiN coating on biomedical AISI 316L stainless steel*, Surface and Coating Technology, Vol. 200, No. 12-13, pp. 4011-4016, 2006.
- [8] V.H.V. Sarmento, M.G. Schiavetto, P. Hammer, A.V. Benedetti, C.S. Fugivara, P.H. Suegama, S.H. Pulcinelli, C.V. Santilli: *Corrosion protection of stainless steel by polysiloxane hybrid coatings prepared using the sol-gel process*, Surface and Coating Technology, Vol. 204, No. 16-17, pp. 2689-2701, 2010.
- [9] P. Misaelides, A. Hatzidimitriou, F. Noli, A.D. Pogrebnjak, Y.N. Tyurin, S. Kosionidis: *Preparation, characterization, and corrosion behavior of protective coatings on stainless steel samples deposited by plasma detonation techniques*, Surface and Coatings Technology, Vol. 180-181, pp. 290-296, 2004.
- [10] R. Di Maggio, L. Fedrizzi, S. Rossi, P. Scardi: *Dry and wet corrosion behaviour of AISI 304 stainless steel coated by sol-gel ZrO₂ CeO₂ films*, Thin Solid Films, Vol. 286, No. 1-2, pp. 127-135, 1996.
- [11] C. Wang, F. Jiang, F. Wang: *The characterization and corrosion resistance of cerium chemical conversion coatings for 304 stainless steel*, Corrosion Science, Vol. 46, No. 1, pp. 75-89, 2004.
- [12] C.R. Tomachuk, C.I. Elsner, A.R. Di Sarli, O.B. Ferraz: *Corrosion resistance of Cr (III) conversion treatments applied on electrogalvanised steel and subjected to chloride containing media*, Materials Chemistry and Physics, Vol. 119, No. 1-2, pp. 19-29, 2010.
- [13] D. Pech, P. Steyer, J. P. Millet: *Electrochemical behaviour enhancement of stainless steels by a SiO₂ PACVD coating*, Corrosion Science, Vol. 50, No. 5, pp. 1492-1497, 2008.
- [14] J. Kawakita, T. Fukushima, S. Kuroda, T. Kodama: *Corrosion behaviour of HVOF sprayed SUS316L stainless steel in seawater*, Corrosion Science, Vol. 44, No. 11, pp. 2561-2581, 2002.
- [15] C.X. Li, T. Bell: *Corrosion properties of plasma nitrided AISI 410 martensitic stainless steel in 3.5% NaCl and 1% HCl aqueous solutions*, Corrosion Science, Vol. 48, No. 8, pp. 2036-2049, 2006.
- [16] C.X. Shan, X. Hou, K. L. Choy: *Effects of pre-sputtered Al interlayer on the atomic layer deposition of Al₂O₃ films on Mg-10Li-0.5 Zn alloy*, Surface & Coatings Technology, Vol. 202, pp. 2399-2402, 2008.
- [17] E. Marin, L. Guzman, A. Lanzutti, W. Ensinger, L. Fedrizzi: *Multilayer Al₂O₃/TiO₂ Atomic Layer Deposition coatings for the corrosion protection of stainless steel*, Thin Solid Films, Vol. 522, pp. 283-288, 2012.
- [18] P. Corengia, F. Walther, G. Ybarra, S. Sommadossi, R. Corbari, E. Broitman: *Friction and rolling-sliding wear of DC-pulsed plasma*

- nitrided AISI 410 martensitic stainless steel*, *Wear*, Vol. 260, No. 4-5, pp. 479-485, 2006.
- [19] C. Ould, X. Badiche, P. Montmitonnet, Y. Gachon: *PVD coated mill rolls for cold rolling of stainless steel strips—Tribological and mechanical laboratory tests*, *Journal of Manufacturing Processes*, Vol. 15, No. 1, pp. 77-86, 2012.
- [20] J.B. Cambon, F. Ansart, J.P. Bonino, V. Turq: *Effect of cerium concentration on corrosion resistance and polymerization of hybrid sol-gel coating on martensitic stainless steel*, *Progress in Organic Coatings*, Vol. 75, No. 4, pp. 486-493, 2012.
- [21] M.A. Chowdhury, D.M. Nuruzzaman: *Experimental Investigation on Friction and Wear Properties of Different Steel Materials*, *Tribology in Industry*, Vol. 35, No. 1, pp. 42-50, 2013.
- [22] T. Suntola, J. Antson, U.S. Patent 4058430, 1977.
- [23] T. Suntola: *On the mechanism of switching effects in chalcogenide thin films*, *Solid State Electron*, Vol. 14, No. 10, pp. 933-938, 1971.
- [24] T. Stubb, T. Suntola, O.J.A. Tiainen: *High field effects in chalcogenide thin films*, *Solid State Electron*, Vol. 15, No. 6, pp. 611-616, 1972.
- [25] T. Suntola, O.J.A. Tiainen, M. Valkiainen: *Frequency-dependent conductivity and capacitance in chalcogenide thin films*, *Thin Solid Films*, Vol. 12, No. 2, pp. 227-230, 1972.
- [26] T. Suntola: *Atomic Layer Epitaxy*, *Thin Solid Films*, Vol. 216, No. 1, pp. 84-89, 1992.
- [27] M. Ahonen, M. Pessa, T. Suntola: *A study of ZnTe films grown on glass substrates using an atomic layer evaporation method*, *Thin Solid Films*, Vol. 65, No. 3, pp. 301-307, 1980.
- [28] J. Lua, J. Aarik, J. Sundqvist, K. Kukli, A. Harsta, J.O. Carlsson: *Analytical TEM Characterization of the Interfacial Layer Between ALD HfO₂ Film and Silicon Substrate*, *J. Cryst. Growth*, Vol. 273, No. 3-4, pp. 510-514, 2005.
- [29] S.M. Bedair, *The Encyclopedia of Advanced Materials*, vol 1. Edited by Bloor D, Brook RS, Flemings, M.C., Mahajan, S., Oxford: Pergamon 141, 1994.
- [30] R. Matero, M. Ritala, M. Leskelä, T. Salo, J. Aromaa, O. Forsén, *J. Phys. IV France* 09, 493, 1999.
- [31] C.X. Shan, X. Hou, K. L. Choy: *Improvement in corrosion resistance of CrN coated stainless steel by conformal TiO₂ deposition*, *Surf. Coat. Technol.*, Vol. 202, No. 10, 2147-2151, 2008.
- [32] E. Marin, A. Lanzutti, L. Guzman, L. Fedrizzi: *Corrosion protection of AISI 316 stainless steel by ALD alumina/titania nanometric coatings*, *Coat. Technol. Res.*, Vol. 8, No. 5, pp. 655-659, 2011.
- [33] E. Härkönen, B. Diaz, J. Światowska, V. Maurice, A. Seyeux, M. Vehkamäki, T. Sajavaara, M. Fenker, P. Marcus, M. Ritala: *Corrosion protection of steel with oxide nanolaminates grown by atomic layer deposition*, *J. Electrochem. Soc.*, Vol. 158, No. 11, pp. 369-378, 2011.
- [34] M. Ritala: *Advanced ALE processes of amorphous and polycrystalline films*, *Appl. Surf. Sci.*, Vol. 112, pp. 223-230, 1997.
- [35] J. Takadom, H.H. Bennani: *Influence of substrate roughness and coating thickness on adhesion, friction and wear of TiN films*, *Surf. Coat. Technol.*, Vol. 96, No. 2-3, pp. 272-282, 1997.
- [36] H.C. Barshilia, A. Ananth, J. Khan, G. Srinivas: *Ar+ H₂ plasma etching for improved adhesion of PVD coatings on steel substrates*, Vol. 86, No. 8, pp. 1165-1173, 2012.
- [37] A. Lanzutti, M. Lekka, E. Marin, L. Fedrizzi: *Tribological Behavior of Thermal Spray Coatings, Deposited by HVOF and APS techniques, and composite electrodeposits Ni/SiC at both room temperature and 300 °C*, *Tribology in Industry*, Vol. 35, No. 2, pp. 113-122, 2013.
- [38] R. Payling, D.G. Jones and A. Bengtson: *"Glow Discharge Optical Emission Spectrometry"*, John Wiley, Chichester, 1997.